Journal of Geographic Information System, 2026, 18(6), 310-333
https://www.scirp.org/journal/jgis
ISSN Online: 2151-1969
ISSN Print: 2151-1950

A Geospatial-SEIRD Framework for Modeling Potential Ebola Dissemination in Uganda

Toluwanimi Grace Akinwande[1], Maria Assumpta Komugabe[2*], Itamar Shabtai[2], Moses Kizito[3], Conrad Shayo[4]

[1]Institute of Mathematical Science, Claremont Graduate University, Claremont, CA, USA
[2]Center for Information Systems and Technology, Claremont Graduate University, Claremont, CA, USA
[3]Ministry of Health Uganda, Department of Planning, Financing and Policy, Division of Health Information Management Uganda, Kampala, Uganda
[4]Department of Information and Decision Sciences, California State University, San Bernardino, CA, USA
Email: toluwanimi.akinwande@cgu.edu, *maria-assumpta.komugabe2@cgu.edu, Itamar.Shabtai@cgu.edu, kztmoz@gmail.com, CShayo@csusb.edu

How to cite this paper: Akinwande, T.G., Komugabe, M.A., Shabtai, I., Kizito, M. and Shayo, C. (2026) A Geospatial-SEIRD Framework for Modeling Potential Ebola Dissemination in Uganda. *Journal of Geographic Information System*, **18**, 310-333.
https://doi.org/10.4236/jgis.2026.186017

Received: October 13, 2026
Accepted: November 23, 2026
Published: November 26, 2026

Copyright © 2026 by author(s) and Scientific Research Publishing Inc.
This work is licensed under the Creative Commons Attribution International License (CC BY 4.0).
http://creativecommons.org/licenses/by/4.0/
Open Access

Abstract

This study develops a Geospatial-SEIRD metapopulation framework to examine potential Ebola Virus Disease dissemination from eastern Democratic Republic of the Congo into Uganda. The model integrates compartmental disease dynamics with Geographic Information Systems, connectivity of the transport network, distance-based mobility weighting, and risk of cross-border exposure to assess spatial transmission in ten Ugandan districts. Epidemiological data were used to initialize susceptible, exposed, infectious, recovered, and deceased compartments, while parameter uncertainty was evaluated through bootstrap estimation of the transmission rate. Network analysis identified Kampala/Wakiso as a major national transportation hub and highlighted western and northwestern border districts, including Kasese, Bundibugyo, Ntoroko, Kisoro, Arua, Nebbi, and Hoima, as important potential entry and dissemination corridors. Baseline simulations showed that, under the estimated low transmission rate, infections remain sub-threshold and decline toward clearance without sustained inter-district spread. The framework provides a spatially informed decision-support tool for prioritizing surveillance and targeted public health interventions in highly connected districts. The analysis is restricted to recognizable and mapped transportation routes available in the dataset and does not account for informal porous border crossings or districts with insufficient route clarity.

Keywords

Geospatial-SEIRD, Metapopulation, Transmission, Ebola, Uganda

1. Introduction

Ebola disease is a highly infectious, acute, and often fatal hemorrhagic illness caused by viruses within the Orthoebolavirus genus of the Filoviridae family [1]. According to the World Health Organization [2], this pathogen represents one of the world's most dangerous viral infections, carrying an average case fatality rate of approximately 50%, with historical outbreaks exhibiting mortality rates ranging from 25% to 90% depending on the specific viral species and local clinical infrastructure. The virus is inherently zoonotic, with fruit bats of the Pteropodidae family serving as the primary natural reservoir hosts [2]. Spillover events into human populations occur through close contact with the blood, secretions, organs, or other bodily fluids of infected wild animals, such as non-human primates (including gorillas, chimpanzees, and monkeys) and forest antelopes. Once introduced into human populations, the Centers for Disease Control and Prevention (CDC) notes that transmission shifts to human-to-human pathways via direct contact with the blood, feces, vomit, or other bodily fluids of a symptomatic individual, or through indirect contact with fomites and environmental surfaces contaminated with these fluids [3]. Symptom onset typically manifests after an incubation period of 2 to 21 days, beginning abruptly with "dry" systemic symptoms including severe fever, debilitating muscle pain, headaches, and a sore throat [2]. As the disease advances, it progresses to "wet" gastrointestinal clinical features such as vomiting, diarrhea, and a rash, alongside impaired kidney and liver function. In severe, late-stage clinical presentations, patients experience internal and external hemorrhaging—such as bleeding from the gums, nose, or gastrointestinal tract—culminating in multi-organ failure, severe fluid loss, and fatal metabolic shock. The lack of licensed vaccines or targeted medical countermeasures for rarer filovirus species, coupled with rapid viral replication, makes the pathogen a severe threat to global health security and underscores the absolute necessity of predictive containment modeling.

1.1. Background and Motivation

The declaration of a Bundibugyo Ebola virus disease (BVD) outbreak in the Democratic Republic of the Congo (DRC) on 15 May 2026, followed by the confirmation of an imported case in Uganda, highlighted the continued threat of cross-border infectious disease transmission in East Africa. The rapid escalation of the outbreak prompted the World Health Organization (WHO) to declare a Public Health Emergency of International Concern (PHEIC) on 17 May 2026 due to the growing risk of regional and international spread [4] [5]. The outbreak has been concentrated in eastern DRC, particularly in Ituri, North Kivu, and South Kivu Provinces, with confirmed cross-border transmission reported in Uganda. As of 3 June 2026, the DRC had reported 344 confirmed cases and 60 deaths, while Uganda had recorded 15 confirmed cases and one death linked to travel-associated and local transmission [6]. The spread of infections across national borders underscores the importance of understanding how population mobility, transpor-

tation networks, conflict, displacement, and porous borders influence disease transmission dynamics.

Bundibugyo ebolavirus remains a significant public health concern because, unlike the Zaire strain, there are currently no licensed vaccines, therapeutics, or rapid diagnostic tools specifically developed for this species [7]. Consequently, outbreak control relies heavily on surveillance, contact tracing, border health measures, and rapid public health response [8]. The 2026 outbreak therefore provides an important opportunity to examine how Ebola may spread through interconnected transportation networks and to identify locations where surveillance and preparedness interventions can be prioritized. This study applies a Geospatial-SEIRD framework integrated with Geographic Information Systems (GIS) and transportation-network analysis to investigate potential Ebola transmission pathways between eastern DRC and Uganda. By combining epidemiological concepts with spatial connectivity analyses, the study aims to identify vulnerable districts, major dissemination corridors, and urban amplification nodes that may facilitate regional disease spread.

As of June 2026, the DRC had reported hundreds of confirmed and suspected Ebola cases concentrated in Ituri, North Kivu, and South Kivu Provinces, with imported cases reported in Uganda. The outbreak occurred within a region affected by conflict, population displacement, and porous borders, creating significant challenges for surveillance and containment [6] [9]. The International Organization for Migration (IOM) has emphasized that mobility restrictions alone are insufficient for outbreak control because they may divert movement toward informal crossings where surveillance is limited. These conditions highlight the importance of understanding transportation networks and cross-border mobility pathways in shaping Ebola transmission dynamics.

1.2. Related Literature

Traditional mathematical frameworks for tracking EVD transmission frequently face limitations in predictive robustness due to a general neglect of pathogen spatial variability across fragmented landscapes [10]. Conventional models rarely evaluate how interconnected natural and anthropogenic factors simultaneously influence host spatiotemporal movement, making it difficult for public health entities to accurately differentiate between active outbreak source and sink zones [10]. Similarly, historic multi-criteria decision analysis methods integrated with geographic information systems (GIS) are often constrained by restricted geographic scales and unextendable architectures [11]. Recent advancements utilizing macro-scale Species Distribution Models, such as Maximum Entropy (MaxEnt), have partially countered these limitations by demonstrating that EVD geographic suitability is heavily driven by human population density, annual rainfall, and temperature seasonality—pinpointing highly vulnerable transmission hubs concentrated primarily across Western and Central Africa, alongside localized risk zones in Eastern Africa [11].

Uganda's close geographic proximity to endemic zones has historically generated acute cross-border transmission risks requiring localized vulnerability tracking. During the 2018 epidemic in the Democratic Republic of the Congo (DRC), Uganda's Ministry of Health integrated the WHO Consolidated Preparedness Checklist with CDC Border Health and Population Connectivity Across Borders (PopCAB) toolkits to map 40 official and unofficial ground crossings and over 500 highly connected locations [1]. While this baseline assessment exposed severe systemic gaps—revealing that 10 of the 12 priority border districts scored below 50.

Controlling Bundibugyo ebolavirus presents an exceptional public health crisis because, unlike the Zaire ebolavirus strain, there are currently no licensed vaccines, targeted therapeutics, or rapid diagnostic tools specifically developed for this species [7]. Consequently, containment is entirely reliant on non-pharmaceutical interventions: syndromic surveillance, border screening, contact tracing, and rapid localized containment. The International Organization for Migration (IOM) has emphasized that unilateral mobility restrictions alone are insufficient, as strict enforcement often diverts human movement toward unmonitored informal crossings where public health screening is entirely absent [9]. This ongoing outbreak provides an imperative operational window to examine exactly how Ebola moves through interconnected transportation networks.

Traditional modeling applications are typically restricted to isolated, stationary populations using a closed Susceptible-Exposed-Infectious-Recovered and Death (SEIRD) setup. By leveraging macro-level transportation network analysis, this study mathematically introduces vector and host movement across localized boundaries. This network-driven expansion converts the static framework into a dynamic SEIRD model that captures transmission, geographic relocation, and infection-induced mortality (D) across connected infrastructural hubs. By coupling compartmental epidemiological mechanics with spatial connectivity analyses, this framework seeks to answer the research question:

Which Ugandan border districts are most exposed to active outbreak locations in eastern DRC?

2. Methodology of the Dynamics of Ebola Virus Disease (EVD) Spread

Unlike a conventional SEIR model that assumes a homogeneous population, the proposed Geospatial-SEIRD framework incorporates transportation-network connectivity derived from GIS analyses and environmental risk factors associated with zoonotic spillover. Network-derived mobility pathways influence spatial transmission between districts, while ecological variables modify local exposure risk. To account for the spatial spread of Ebola Virus Disease (EVD) between geographically distinct regions, we extend the classical SEIR model into a geo-spatial metapopulation framework. The total population is partitioned into n districts, each represented by five epidemiological compartments: susceptible (S_i), exposed (E_i), infectious (I_i), recovered (R_i), and deceased (D_i), where $i = 1, \cdots, n$.

The total living population in district i at time t is given by

$$N_i(t) = S_i(t) + E_i(t) + I_i(t) + R_i(t). \quad (1)$$

conserving population across the network. The deceased compartment is excluded from the population at risk since deceased individuals do not contribute to population mixing. Although, funeral and burial of deceased ebola victims can propagate the transmission of the ebola virus disease, we do not consider this in this study, we particularly focus on the dynamics of geospatial spread of the ebola virus between a many districts. We also do not factor in particular vaccination effect, clinical treatment interventions or targeted isolation in our model.

2.1. Disease Transmission Dynamics

Susceptible individuals become exposed through effective contact with infectious individuals within the same district. The force of infection in district i is given by

$$\lambda_i(t) = \beta \frac{I_i(t)}{N_i(t)},$$

where β denotes all district's transmission rate [12].

Exposed people progress to the infectious class at rate σ, corresponding to an average incubation period of $1/\sigma$ days. Infectious individuals either recover at rate γ or die due to the disease at rate μ. Consequently, the average infectious period is

$$\frac{1}{\gamma + \mu}.$$

[13].

2.2. Mobility Structure

People mobility between districts is represented by a mobility matrix

$$M = \left(m_{ij}\right)_{n \times n},$$

where m_{ij} denotes the per-capita movement rate from district i to district j.

The corresponding mobility operator is defined as $L = M^{\mathrm{T}} - D$ where

$$D = \operatorname{diag}\left(\sum_{j=1}^{n} m_{1j}, \sum_{j=1}^{n} m_{2j}, \cdots, \sum_{j=1}^{n} m_{nj}\right).$$

So for any state vector $X = \left(X_1, \cdots, X_n\right)^{\mathrm{T}}$, the term $\left(LX\right)_i$ represents the net movement into each district, yielding:

$$\left(LX\right)_i = \sum_{j=1}^{n} m_{ji} X_j - \sum_{j=1}^{n} m_{ij} X_i.$$

[14].

2.3. Compartment-Specific Mobility

Since mobility behavior is different among epidemiological states, we assign sep-

arate mobility operators to each compartment. Susceptible, exposed, and recovered individuals are assumed to travel according to the baseline mobility pattern,

$$L_S = L_E = L_R = kL. \tag{2}$$

where k is the mobility coefficient $k \in [0,1]$. Infectious individuals experience substantially reduced mobility due to symptoms, hospitalization or isolation measures. Their mobility operator is defined as

$$L_I = \alpha L, \quad 0 \le \alpha \le 1,$$

where α denotes the infectious mobility reduction factor. Deceased individuals are assumed immobile and therefore

$$L_D = 0.$$

2.4. Model Equations

The system of ordinary differential equations governing the geospatial SEIRD model for each district i is given by:

$$\frac{\mathrm{d}S_i}{\mathrm{d}t} = -\beta \frac{S_i I_i}{N_i} + \sum_{j=1}^{n} m_{ji} S_j - \sum_{j=1}^{n} m_{ij} S_i,$$

$$\frac{\mathrm{d}E_i}{\mathrm{d}t} = \beta \frac{S_i I_i}{N_i} - \sigma E_i + \sum_{j=1}^{n} m_{ji} E_j - \sum_{j=1}^{n} m_{ij} E_i,$$

$$\frac{\mathrm{d}I_i}{\mathrm{d}t} = \sigma E_i - (\gamma + \mu) I_i + \alpha \left(\sum_{j=1}^{n} m_{ji} I_j - \sum_{j=1}^{n} m_{ij} I_i \right),$$

$$\frac{\mathrm{d}R_i}{\mathrm{d}t} = \gamma I_i + \sum_{j=1}^{n} m_{ji} R_j - \sum_{j=1}^{n} m_{ij} R_i,$$

$$\frac{\mathrm{d}D_i}{\mathrm{d}t} = \mu I_i.$$

[14] and hence we present the system across the entire network compactly. Let

$$S = (S_1, \cdots, S_n)^{\mathrm{T}}, \quad E = (E_1, \cdots, E_n)^{\mathrm{T}}, \quad I = (I_1, \cdots, I_n)^{\mathrm{T}},$$
$$R = (R_1, \cdots, R_n)^{\mathrm{T}}, \quad D = (D_1, \cdots, D_n)^{\mathrm{T}}.$$

Define the network-wide infection vector F using the Hadamard product notation:

$$F = \beta \frac{S \odot I}{N},$$

where $\odot$ denotes element-wise multiplication. The model equations can then be written compactly in vector form as:

$$\frac{\mathrm{d}S}{\mathrm{d}t} = -F + LS,$$

$$\frac{\mathrm{d}E}{\mathrm{d}t} = F - \sigma E + LE,$$

$$\frac{\mathrm{d}I}{\mathrm{d}t} = \sigma E - (\gamma + \mu) I + \alpha L I,$$

$$\frac{\mathrm{d}R}{\mathrm{d}t} = \gamma I + LR,$$

$$\frac{\mathrm{d}D}{\mathrm{d}t} = \mu I.$$

with the initial conditions at $t = 0$:

$$S_i(0) = S_{i0},\ E_i(0) = E_{i0},\ I_i(0) = I_{i0},\ R_i(0) = R_{i0},\ D_i(0) = D_{i0}.$$

These initial compartments satisfy the total initial network constraints:

$$N_i(0) = S_{i0} + E_{i0} + I_{i0} + R_{i0} + D_{i0}.$$

The initial exposed, infectious, dead and recovered populations are estimated from surveillance records.

2.5. Mobility Process in a Metapopulation Network

The spatial spread of Ebola is modeled using a metapopulation framework in which each district is represented as a node in a directed network and population movement between districts occurs along the network edges. Such metapopulation models have been widely used to study the spread of infectious diseases across geographically separated populations [14] [15].

Let $G = (V, E)$ denote a directed graph whose vertices correspond to districts and whose edges represent movement routes between districts. For each pair of connected districts i and j, let d_{ij} denote the road distance between the two locations. Due to incomplete empirical traffic-flow data we assume mobility decrease with increasing distance according to a distance-decay relationship. To incorporate the underlying transportation network structure, let $A = (A_{ij})$ denote the adjacency matrix of the directed graph, where

$$A_{ij} = \begin{cases} 1, & \text{if a direct connection exists between districts } i \text{ and } j, \\ 0, & \text{otherwise.} \end{cases}$$

Let d_{ij} denote the distance matrix, where d_{ij} is the road distance between districts i and j. Following the heterogeneous diffusion framework proposed by Colizza and Vespignani [14] [15], a weighted network is constructed by assigning each edge a weight

$$w_{ij} = A_{ij} \frac{1}{d_{ij}^{\eta}},$$

where $\eta > 0$ is a distance-decay exponent controlling the influence of distance on mobility. In this study, we set $\eta = 1$ for simplicity, yielding weights that are inversely proportional to the distance between connected districts. Consequently, districts connected by shorter routes are assigned larger edge weights and are therefore assumed to experience greater mobility interactions than districts separated by longer distances. The adjacency matrix A is a matrix of ones, since all districts are connected to each other as shown in **Figure 3**.

For each district i, the total outgoing traffic strength is defined as $s_i = \sum_j w_{ij}$, which represents the aggregate connectivity of district i within the transporta-

tion network. The mobility rate from district i to district j is then defined by normalizing the edge weights,

$$m_{ij} = \frac{w_{ij}}{\sum_{\ell} w_{i\ell}} = \frac{w_{ij}}{s_i}, \tag{3}$$

The resulting mobility matrix is $M = \left[m_{ij} \right]$, whose entries quantify the rate at which individuals leave a district to another.

2.6. State and Parameter Definition

Figure 1 shows the epidemic state compartments and the transition processes between them.

The fixed biological parameter configurations were derived from historical filovirus outbreak literature, fixing the transition rate out of the latent class at $\sigma = 1/5.3 \text{ day}^{-1}$, representing a mean incubation period of 5.3 days [16]. The disease mortality rate was set at $\mu = 0.10 \text{ day}^{-1}$ based on reported institutional mortality indices [13]. We formulate the recovery rate (γ) as a function of the total infectious clearance rate and the disease-induced mortality as:

$$\gamma = \frac{1}{P_{\text{inf}}} - \mu = \frac{1}{5.61} - 0.10 \approx 0.07825 \text{ day}^{-1} \tag{4}$$

thereby strictly anchoring the mean infective period to $P_{\text{inf}} = 5.61$ days [12] [17]. Table 1 and Table 2 provide definitions of the parameters used in the model.

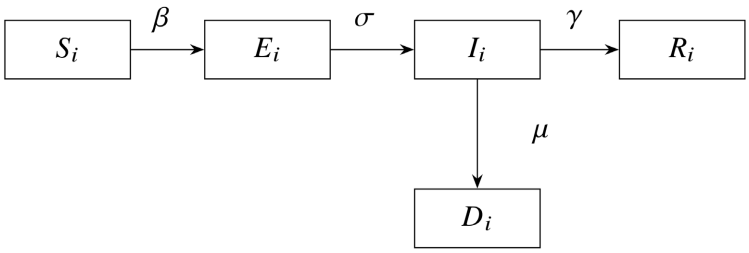


Figure 1. Compartmental structure of the district-level metapopulation SEIRD model. Individuals progress from susceptible (S_i) to exposed (E_i), infectious (I_i), recovered (R_i), or deceased (D_i).

Table 1. Description of model parameters.

Parameter	Units	Description
β	day^{-1}	Transmission rate across districts
σ	day^{-1}	Progression rate from exposed to infectious
γ	day^{-1}	Recovery rate
μ	day^{-1}	Disease-induced mortality rate
m_{ij}	day^{-1}	Movement rate from district i to district j
α	dimensionless	Mobility reduction factor for infectious individuals
L	day^{-1}	Mobility operator $M^{\mathrm{T}} - D$

Table 2. Baseline parameter values used in simulations.

Parameter	Value	Source	Interpretation
σ	1/5.3	Literature	Mean incubation period of 5.3 days
γ	0.078	Literature	Recovery rate
μ	0.10	Inferred	Disease mortality rate
α	0.10	Literature	Infectious individuals travel at 10% of normal mobility

2.7. Epidemiological Data Processing

Due to severe constraints regarding detailed clinical compartmental timelines within the Democratic Republic of the Congo (DRC), the cross-border epidemic is not modeled as an explicit, parallel multi-district dynamic system. Furthermore, according to public health directives and regional reporting, Ugandan management enacted a temporary cessation of routine cross-border movement, restricting border passage exclusively to specialized emergency response teams [18]. Therefore, we do not model inter-country transmission dynamics as a continuous, time-dependent dynamic influx function. Instead, the cumulative cross-border infections that occurred prior to the border closure are entirely infused directly into the baseline state of the latent, unobserved exposed state ($E_i(0)$). This static cross-border seeding approach is evaluated at the reference baseline date (t_0 = June 10, 2026). This section outlines the structural processing of empirical case data, the sorting of localized versus imported vectors.

Epidemiological reporting as of June 10, 2026, provides stratified pairs of values for Ugandan districts: case matrices capturing strictly localized transmission, and expanded registries including cumulative introductions from the DRC [4] [6]. Let I_i^{local}, R_i^{local}, and D_i^{local} define the localized active infectious, recovered, and deceased populations within district i, respectively. Let I_i^{total}, R_i^{total}, and D_i^{total} represent the total cumulative counts including imported vectors.

The baseline states for the manifest compartments—Infectious ($I_i(0)$), Recovered ($R_i(0)$), and Deceased ($D_i(0)$)—are explicitly initialized using the total empirical observation vectors: $I_i(0) = I_i^{\text{total}}$ $R_i(0) = R_i^{\text{total}}$ $D_i(0) = D_i^{\text{total}}$. The exact number of imported cases per district (Λ_i) is structurally determined by filtering localized noise from the total raw contacts data across all compartments: $\Lambda_i = \left(I_i^{\text{total}} - I_i^{\text{local}}\right) + \left(R_i^{\text{total}} - R_i^{\text{local}}\right) + \left(D_i^{\text{total}} - D_i^{\text{local}}\right)$. Evaluating the empirical data yields $\sum_{i=1}^{10} \Lambda_i = 14$ total cross-border index importations distributed exclusively among two critical primary transmission hubs: Kampala and Wakiso as displayed in **Table A1**. All remaining eight districts are anchored at zero initial clinical manifestation. The ten chosen Ugandan districts are chosen because of their proximity to the DRC epicenters.

Estimation of Exposed Class

Although clinical compartments (I, R, D) are completely defined by localized surveillance data, the exposed latent, unobserved class (E) is given only as an

aggregate of national raw contact data from contact-tracing records. To prevent modeling over-fit caused by introducing raw tracking raw contacts data directly as biological exposures, the total initial latent exposed volume across the entire network (E_{total}) is scaled downward using an empirical conversion efficiency multiplier (ω):

$$E_{\text{total}} = \Omega_{\text{contacts}} \times \omega \tag{5}$$

where Ω_{contacts} represents the total unassigned contact data extracted from the raw datasets, and ω acts as the transmission efficiency scalar representing the statistical probability of a tracked contact transitioning into a valid pathologically incubated state. Building on established filovirus outbreak literature regarding household and community secondary attack rates (SAR) [19] [20], ω is strictly constrained to the interval $\omega \in [0.05, 0.12]$ to prevent artificial over-seeding of the latent compartment from unverified contact registries. This parameter configuration is anchored directly to empirical secondary attack rates (SAR) observed in community and household line-lists during historical Sudan and Bundibugyo ebolavirus outbreaks [21] [22]. Restricting ω to this range mathematically preserves the biological logic of the model, preventing an artificial inflation or "over-seeding" artifact in the exposed class which would otherwise generate a massive, mathematically unrealistic wave of active symptomatic cases (I_i) within a single incubation cycle [13].

Since cross-border case arrival is treated as a single initialization infusion rather than a continuous function of time due to the border control mandates, a hybrid mathematical allocation index (W_i) is formulated to map exposures across the 10 Ugandan districts. This index balances two separate epidemiological drivers: the historical risk of undetected cross-border infiltration prior to boundary restrictions and the localized contact density generated by known, active domestic cases.

The cross-border introduction hazard is modeled as an inverse-distance power function relative to the five major active DRC epicenter hubs (Bunia, Mongbwalu, Beni, Butembo, and Goma) [4] [23]. For each Ugandan district i, the geographic risk weight p_i is expressed as:

$$p_i = \frac{G_i}{\sum_{j=1}^{10} G_j} \text{ where } G_i = \sum_{r=1}^{5} d_{ri}^{-\eta}$$

Here, d_{ri} represents the geodesic distance (km) from DRC epicenter r to Ugandan destination patch i as shown in **Table A2**, and $\eta \geq 1$ is the distance friction parameter optimizing spatial drop-off behavior.

Internal secondary transmission risks scale proportionally to local prevalence. The internal contact generation weight is derived directly from the ratio of active symptomatic vectors present in a given district:

$$V_i = \frac{I_i(0)}{\sum_{j=1}^{10} I_j(0)}$$

Blending the cross-border introduction hazard with domestic cases density via an adjustment weight $w \in [0,1]$ yields the definitive spatial risk distribution function:

$$W_i = wp_i + (1-w)V_i$$

So, the initial conditions for the unobserved exposed state $E_i(0)$ across all 10 Ugandan patches are initialized as:

$$E_i(0) = E_{\text{total}} \times \frac{W_i}{\sum_{j=1}^{10} W_j} \tag{6}$$

To enforce strict conservation of total mass across the multi-patch metapopulation network, the initial completely susceptible pool ($S_i(0)$) for each discrete district is resolved by subtracting all non-susceptible conditions from the census population baseline $N_i : S_i(0) = N_i - E_i(0) - I_i(0) - R_i(0) - D_i(0)$, with populations given in **Table A3**. This framework reconciles unassigned regional data streams in the DRC, grounding the network model in structural geographic boundaries without relying on time-dependent cross-border dynamic dependencies.

This study relies on available and recognizable transportation-route data derived from the mapped road network. Consequently, the model does not capture informal porous border crossings, undocumented mobility pathways, or districts for which route connectivity was unclear or insufficiently represented in the available data, such as Kanungu District. Therefore, the findings should be interpreted as estimates based on observable and data-supported mobility routes rather than a complete representation of all possible cross-border movements.

2.8. Transmission Rate Estimation

To estimate the daily transmission rate (β) for the 2026 sub-national ebolavirus outbreak in Uganda, we calibrated the deterministic multi-district SEIRD system against cumulative incidence snapshots spanning from May 15 to June 13, 2026. [4] [6], as shown in **Table A4**. The surveillance observations are newly reported cases at two-day intervals, beginning with three cases on day 0, May 15. To align the discrete observation index with physical time, calendar time was scaled via $t_k = 2 \cdot \text{Day}_k$. For calibration, the incident counts were accumulated to construct the cumulative observations so that parameter estimation is stable against high-frequency testing noise. With:

$$C_k^{\text{obs}} = \sum_{i=1}^{k} \Delta C_i^{\text{obs}}, \quad k \in \{1, \cdots, 14\},$$

accumulating monotonically to $C(26) = 21$ cases on June 10. In this framework, surveillance data lack national level contact tracing identifiers to distinguish imported cross-border cases from locally acquired secondary infections; consequently, all contact tracing data at $t = 0$ are absorbed into the initial seed conditions ($I_0 = 3$, $E_0 = 148 \times 0.08 = 11.84, R_0 = 0 = D_0$), where 148 is the raw contact count and 0.08 is the empirical conversion efficiency multiplier. The transmission coefficient β was estimated using MATLAB's bounded optimization routine,

fminbnd over the bounded interval $\beta \in \left[10^{-6}, 1.5\right]$. The epidemiological parameters were fixed at $\sigma = 1/5.3$, $\gamma = 0.078$, and $\mu = 0.1$. The estimation is governed by a compartmental SEIRD system with an auxiliary cumulative incidence tracker, $\frac{\mathrm{d}C}{\mathrm{d}t} = \sigma E$, solved via a fourth-order Runge-Kutta integrator (ode45) with initial state $\boldsymbol{y}_0 = \left[S_0, E_0, I_0, R_0, D_0, C_0\right]^{\mathrm{T}}$. The point estimate $\hat{\beta}$ is obtained by minimizing the sum of squared errors between cumulative modeled cases $C\left(t;\beta\right)$ and empirical observations $\boldsymbol{C}^{\mathrm{obs}}$,

$$\hat{\beta} = \arg\min_{\beta \in \left[10^{-6}, 1.5\right]} \sum_{i=1}^{k} \left(C\left(t_i;\beta\right) - C_i^{\mathrm{obs}}\right)^2, \text{ where } t \in \left[0, 26\right] \text{ across 26 calendar days.}$$

via golden section search. Due to our small data set, parameter uncertainty is quantified using a parametric Monte Carlo bootstrap through repeated samplings ($B = 1000$ realizations), where synthetic incidence increments are drawn from independent Poisson distributions, parameterized by model-expected incident increments and successively accumulated from baseline C_0 to preserve trajectory monotonicity [24]. Re-optimizing through all $B = 1000$ synthetic realizations yielded an empirical bootstrap sampling distribution characterized by a sample mean of $\overline{\beta} = 0.031780$, a standard deviation of $s_\beta = 0.034456$, and an empirical 95% bootstrap confidence interval of $\left[0.000039, 0.109680\right]$, centered around the point estimate $\hat{\beta} = 0.024881$. The point estimate lies strictly in the interior of the search space ($10^{-6} < \hat{\beta} < 1.5$) and does not reach either optimizer boundary. The basic reproduction number is: $\mathcal{R}_0 = \frac{\hat{\beta}}{\gamma + \mu} = \hat{\beta} \cdot D_{\mathrm{inf}} = 0.024881 \times 5.61 = 0.1396$. This produces a reproductive number $R < 1$, and depicting that transmission chains are not self-sustaining and are unable to generate a major epidemic, showing that the observed case accumulation from 3 to 21 is driven by the deterministic emptying of the initial latent data ($E_0 = 11.84$) rather than sustained secondary community transmission. Also, rather than interpreting the estimate as definitive evidence of negligible transmission, it should be treated cautiously, as it may reflect the small number of observed cases and the assumed initial exposed population.

3. Results and Sensitivity Analysis

3.1. Network Analysis

Democratic Republic of the Congo-Uganda network analysis

Figure 2 illustrates the transportation connectivity between Ebola-affected locations in eastern Democratic Republic of the Congo (DRC) and major transportation hubs in Uganda. The network shows extensive linkages between outbreak locations and Ugandan districts, particularly Kasese, Bundibugyo, Ntoroko, Kisoro, Arua, Nebbi, Hoima, and Kampala/Wakiso. Border districts adjacent to the DRC exhibited the highest concentration of transportation connections, indicating their potential role as primary entry points for cross-border human movement. Kampala/Wakiso emerged as a central transportation hub, connecting multiple

western border districts to the national transportation network. The observed connectivity patterns highlight potential pathways for the movement of travelers between outbreak-affected areas and Uganda, emphasizing the importance of enhanced surveillance, screening, and preparedness efforts in highly connected border districts and major transportation centers to mitigate the risk of cross-border Ebola transmission.

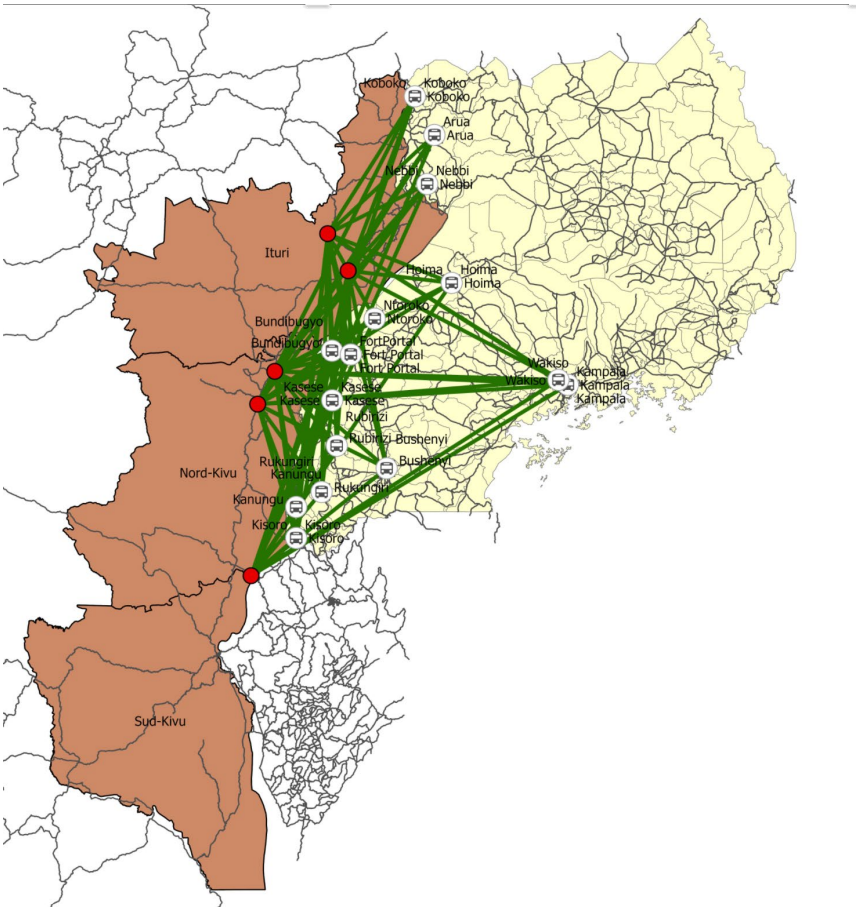


Figure 2. Democratic Republic of Congo-Uganda network analysis. Road network data obtained from ArcGIS Online through ArcGIS Catalog; map created by the author in ArcGIS Pro.

Figure 3 presents the transportation network analysis for districts that had measurable network distances both from and to the selected locations in the study. These districts were included because they were connected through the mapped road transportation network, allowing the analysis to estimate potential movement pathways between outbreak-affected areas and major transit hubs. The results revealed extensive connectivity between Kampala/Wakiso and districts in western and northwestern Uganda, including Kasese, Fort Portal, Hoima, Nebbi, Arua, and Koboko. Kampala/Wakiso emerged as the primary transportation hub, with multiple direct bus connections to outbreak-affected districts. This network demonstrates potential pathways through which routine passen-

ger movement could facilitate the spatial spread of Ebola. Western border districts, particularly Kasese, Fort Portal, and Arua, showed strong transportation linkages with both Kampala and neighboring districts, suggesting a high degree of regional connectivity.

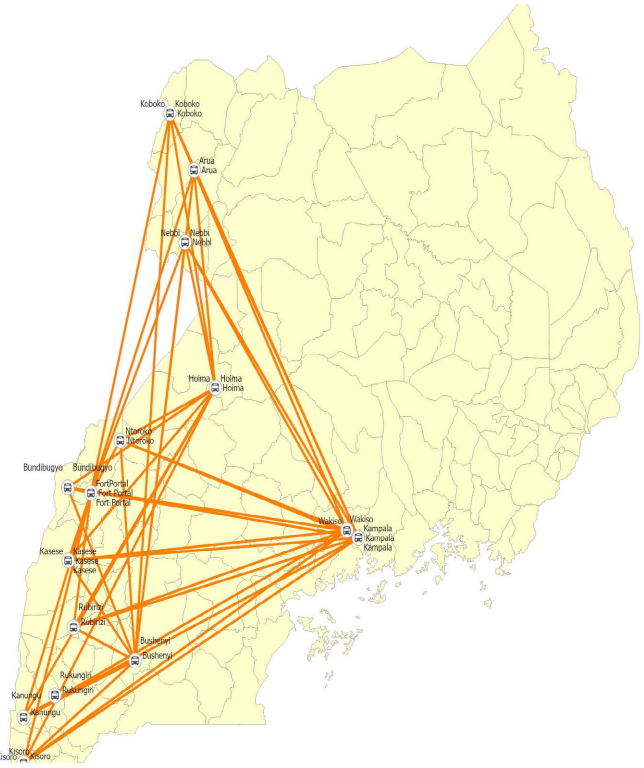


Figure 3. Uganda Transportation network. Road network data obtained from ArcGIS Online through ArcGIS Catalog; map created by the author in ArcGIS Pro.

3.2. Network-Wide Outbreak Dynamics

The continuous spatial progression of Ebola Virus Disease (EVD) across the 10 domestic patches was simulated over a 90-day time horizon. The initial conditions at $t = 0$, which correspond to the June 10 reporting snapshot, were seeded exclusively within the high-density urban corridors of Kampala ($I_1(0) = 9$) and Wakiso ($I_3(0) = 5$), as shown in Table A1. Due to cross-border epidemiological surveillance restrictions and formal border closures between the Democratic Republic of the Congo (DRC) and Uganda, unassigned exposures tracking out of the DRC epicenters (Bunia, Mongbwalu, Beni, Butembo, and Goma) were structurally absorbed into the initial Ugandan exposed class ($E_i(0)$) via a geographic risk weight p_i. with d_{ij} The road distance between Ugandan districts i and j given in Table A5.

As shown in Figure 3, the district network is fully connected, allowing mobility interactions between each pair of districts. This assumption, adopted in the absence of measured passenger-flow data, provides a simplified framework for investigating broad patterns of Ebola dissemination across the selected districts. The domestic

network connectivity matrix was regularized with a baseline mobility coefficient $k = 0.02$ was selected to represent a relatively low level of inter-district mobility and examine disease transmission under such restricted movement. Other mobility intensities will be explored in subsequent simulations to assess how changes in mobility influence the spatial spread of infection. The distance-decay friction exponent $\eta = 1.0$ was chosen so that mobility weights decrease inversely with route distance. The spatial synthesis parameter $w = 0.12$ to blend the risk of cross-border introduction with local population density distributions. To map symptomatic behavioral damping, the active infectious travel multiplier was parameterized at $\alpha = 0.2$, preserving a non-zero travel fraction to capture early-stage prodromal movement before restriction. These assumptions allows us to examine a general investigation of the relationship between parameters such as mobility and disease dissemination but do not represent measured travel behavior. Specifically, although we have a fully connected network, people may not travel between every pair of districts, and distance-based weights cannot exactly capture actual passenger volumes, travel frequency, or route-specific movement patterns. Therefore, disease dissemination pathways should be interpreted as outcomes of hypothetical mobility scenarios rather than precise predictions of actual disease spread. Incorporating observed passenger flows and more realistic travel-network data would improve the model's ability to represent inter-district transmission.

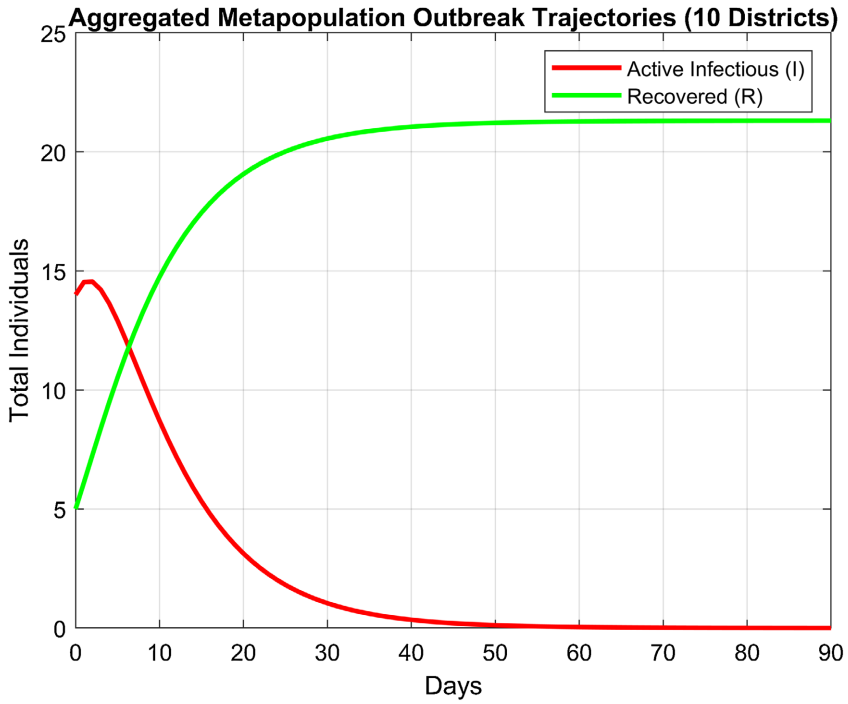


Figure 4. Baseline model trajectories demonstrating rapid clearance of EVD compartments across the network under sub-threshold conditions.

The network-wide aggregated epidemiological trajectories are illustrated in Figure 4. Initialized with an aggregate national burden of 14 active symptomatic

infections and 17.8 latently incubating cases (parameterized under a conservative experimental importation pressure of $\omega = 0.12$), which is derived from a raw contact count of 148. The network-wide infectious profile exhibits a rapid, early peak of approximately 16 active concurrent cases at $t = 4$ days. Given the presence of high-density informal settlements and refugee populations (e.g., Kampala's 149,000 refugees), the probability of a tracked contact transitioning to an active exposure (E) is modeled at a higher threshold to reflect intense localized crowding. Because the estimated transmission coefficient falls strictly below the critical epidemic threshold ($\mathcal{R}_0 \ll 1$), the force of infection is mathematically insufficient to sustain onward community propagation. Consequently, the virus experiences natural extinction, completely clearing the active infectious compartment within approximately 40 days. Concurrently, the exposed state transitions rapidly into the recovery compartment, with the cumulative recovered population stabilizing within few weeks of the timeline.

3.3. Impact of Inter-District Mobility on Spatiotemporal Viral Dispersion

To isolate the explicit structural role of the domestic transportation infrastructure on spatial viral spread, we varied the baseline mobility coupling parameter across an experimental sweep where $k \in [0.00, 1.00]$. The resulting spatiotemporal evolution matrices are visualized via density heatmaps in **Figure 5**.

With careful observation of **Figure 5**, we see that under the completely uncoupled structural configuration ($k = 0.00$), the local outbreaks operate as isolated epidemiological islands. Transmission boundaries remain entirely locked within Kampala and Wakiso, burning out locally through natural recovery and mortality while the remaining eight peripheral destination patches maintain absolute zero-case containment. We observe a subtle diffusion of transmission in Kampala as mobility increases. As the network mobility coefficient scales upward ($k > 0$), because the sub-threshold transmission capacity ($\hat{\beta} = 0.024881$) yields zero localized amplification potential in the target patches, these traveling chains undergo spatial dilution.

Although higher mobility coefficients (up to $k = 1.00$) accelerate inter-district spatial mixing and redistribute cases away from initial epicenters like Kampala and Wakiso to appear in peripheral corridors like Fort Portal, Hoima, and Kasese, these introductions fail to produce sustained secondary transmission chains due to transmission scenarios, thus narrowing their local persistence windows. This lack of onward spread is primarily driven by the fitted transmission parameters ($\hat{\beta} = 0.024881$, $\mathcal{R}_0 < 1$), under which the pathogen lacks the infectious velocity to sustain community transmission. Thus, spatial redistribution across districts does not inherently guarantee clearance or immunity against invasion. Instead, the absence of sustained regional propagation across peripheral districts is a direct consequence of the low transmission rate rather than the population-conserving properties of the metapopulation network.

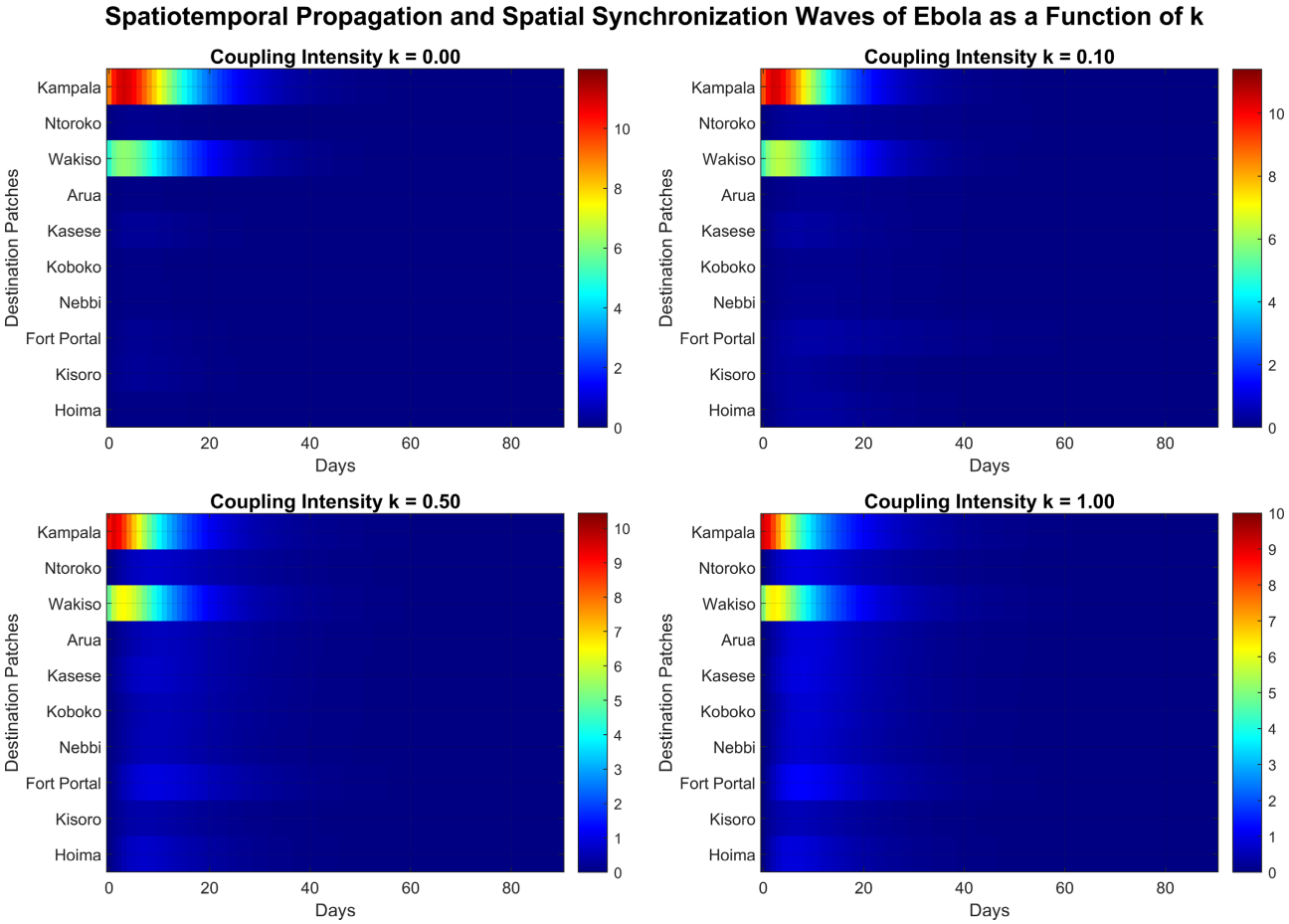


Figure 5. Multi-panel spatiotemporal heatmaps demonstrating localized containment when $k = 0$ and network-wide spatial dilution as $k \to 1$.

3.4. Sensitivity Analysis of Cross-Border Importation Pressure

Finally, we evaluated the sensitivity of the domestic network to cross-border introduction pressure tracking out of the DRC epicenters by sweeping the contact-conversion scale factor over the strict, literature-validated interval of $\omega \in [0.05, 0.12]$. This boundary constraint directly mimics close-contact and household secondary attack rates (SAR) documented across historical Sudan and Bundibugyo ebolavirus outbreaks.

The quantitative results of this sweep are provided in **Figure 6**. Across all evaluated bounds of historical border leakage—ranging from strict filtration ($\omega = 0.05$, initializing $E_{\text{total}} = 7.4$ individuals) to high-exposure leakage ($\omega = 0.12$, initializing $E_{\text{total}} = 17.8$ individuals)—the cumulative propagation profile remains flat. The maximum concurrent case load fails to cross the threshold required to trigger an epidemic trajectory. The outcome metrics consistently support our primary structural findings: the cross-border importation of exposed contacts increases the local baseline initialization volume but cannot alter the underlying sub-threshold thermodynamics of the system. In all simulated configurations, the outbreak follows a uniform decay path toward total clearance,

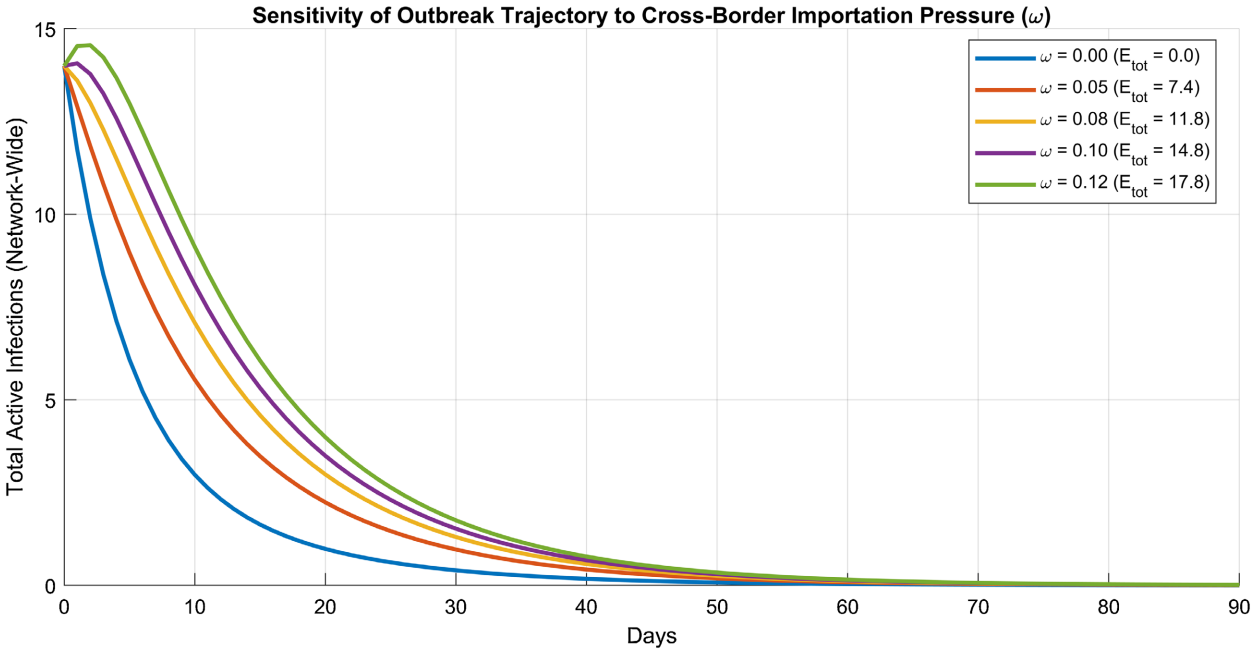


Figure 6. Sensitivity trajectories mapping aggregate infectious curves against variations in cross-border importation scaling constraints.

confirming the robust systemic stability of the Ugandan transportation network under realistic cross-border pressure variations.

4. Discussion

National governments, the World Health Organization (WHO), the International Organization for Migration (IOM), Africa CDC, and numerous humanitarian partners have implemented comprehensive response measures to contain the outbreak. These measures include the deployment of rapid response teams, enhanced laboratory diagnostic capacities, border health screening, infection prevention and control training, community engagement initiatives, and the establishment of dedicated Ebola Treatment Units (ETUs) [4]. Despite these coordinated efforts, systemic challenges remain. A primary operational bottleneck impacting the parameterization of this study is the inconsistency in contact tracing line-lists, which necessitated a mathematical approximation to initialize the latent, exposed class (E_i). This analysis focuses on evaluating the sub-national spatial dispersion dynamics across Uganda's domestic transportation network, given initial cross-border exposure pressures originating from epicenters in the Democratic Republic of the Congo (DRC). Our geospatial SEIRD metapopulation analysis demonstrates that under baseline conditions, the virus lacks sufficient velocity to establish sustained onward transmission across districts due to the highly suppressed estimated transmission rate (β). Our simulation models support the hypothesis that given standard pharmaceutical clinical interventions—such as rapid isolation, targeted treatment, and safe burial practices—the pathogen will naturally transition toward extinction.

This observed responses dictates that healthcare authorities must preemptively stockpile medical countermeasures and personal protective equipment across highly connected hubs, as unrestricted human mobility will broadcast the pathogen rapidly across the sub-national network under high-transmission regimes. These dynamics reveal several critical public health policy insights. First, strengthening national health systems requires sustained financial and structural investments in active surveillance to capture exact contact line-lists, thereby minimizing diagnostic uncertainty in transmission forecasting. Second, effective outbreak control demands highly coordinated regional and inter-district frameworks that account for population mobility. Intervention resources must be strategically deployed to major transportation hubs—such as Kampala and Wakiso—as well as structurally vulnerable transit nodes such as Fort Portal, Kasese, and Hoima.

Limitations and Future Directions

Future extensions of this work will focus on obtaining more robust, real-time surveillance data to estimate district-specific transmission, recovery, and disease-induced mortality rates. furthermore, while our gravity formulation successfully identifies sub-national sub-populations with the highest structural exposure to human movement, the network topology is strictly constrained to formal road transportation infrastructure. Consequently, this model does not account for informal pedestrian border crossings, undocumented mobility pathways, individual behavioral variations or exact passenger traffic volumes.

Additionally, the lack of province-specific, metadata from the DRC necessitated a generalized spatial allocation of imported cases into the initial exposed class. Integrating future inter-country transmission dynamics as a continuous, time-dependent dynamic flux function would significantly refine model fidelity. Therefore, these findings should be interpreted as a structural assessment of potential network connectivity and geographic accessibility rather than direct empirical evidence of active Ebola transmission risk. Despite these limitations, mapping highly connected districts and transportation corridors provides a valuable geographic framework for prioritizing active surveillance, optimizing border screening checkpoints, and guiding community readiness efforts to mitigate cross-border viral spillovers.

5. Conclusions

The 2026 Bundibugyo ebolavirus outbreak in Eastern DRC and its subsequent spillover into Uganda highlights the critical need for coordinated sub-regional and sub-national zoonotic preparedness frameworks. Our metapopulation network analysis demonstrates that while unrestricted human mobility acts as a powerful structural amplifier under high-transmission regimes, the localized velocity of the early-stage 2026 Ugandan clusters was insufficient to overcome geographic dilution and sustain network-wide spatial propagation.

Critically, our findings isolate the specific sub-national patches that demand

heightened active surveillance and preemptive resource allocation during the critical early phase of a high-transmission outbreak. These results also illustrate how missing field registries generate diagnostic uncertainty in core mathematical parameters. However, despite data constraints, our epidemiological simulations consistently verify the robust containment and predictable natural extinguishment of the Bundibugyo virus under baseline conditions, providing clear timelines for pathogen elimination. To optimize future outbreak readiness, national frameworks in resource-constrained settings must prioritize the collection of standardized, high-quality surveillance data. Improving early-stage data integration bridges the gap between mathematical forecasting and field execution, providing public health authorities with informed, actionable strategies for early containment and accelerated disease eradication.

Data Availability Statement

The epidemiological data used in this study were obtained from the Ministry of Health Uganda. Transportation-network data were obtained from ArcGIS Online through ArcGIS Catalog and analyzed in ArcGIS Pro. The analysis is limited to recognizable and mapped transportation routes available in the dataset and does not include informal porous border crossings, undocumented mobility pathways, or districts with insufficient route clarity. Additional data supporting the findings of this study may be made available upon reasonable request after peer review and subject to data-sharing permissions.

Author Contributions

Maria Assumpta Komugabe: Conceptualization, Methodology, Software, Visualization, and Writing—Original Draft.

Toluwanimi Grace Akinwande: Validation, Methodology, Formal Analysis, Visualization, and Writing—Review and Editing.

Kizito Moses: Resources and Data Curation.

Conrad Shayo: Writing—Review and Editing, and Supervision.

Itamar Shabtai: Writing—Review and Editing, and Supervision.

Conflicts of Interest

The authors declare no conflicts of interest regarding the publication of this paper.

References

[1] Nanziri, C., Ario, A.R., Ntono, V., Monje, F., Aliddeki, D.M., Bainomugisha, K., *et al.* (2020) Ebola Virus Disease Preparedness Assessment and Risk Mapping in Uganda, August-September 2018. *Health Security*, **18**, 105-113. https://doi.org/10.1089/hs.2019.0118

[2] World Health Organization (2025) Ebola Disease. WHO Fact Sheet.

[3] Centers for Disease Control and Prevention (2026) Ebola.

[4] World Health Organization (2026) Ebola Disease Caused by Bundibugyo Virus, Dem-

ocratic Republic of the Congo and Uganda. https://www.who.int/emergencies/disease-outbreak-news/item/2026-DON607

[5] Lang, K. (2026) Ebola: What You Need to Know and What to Do about Suspected Cases. *BMJ*, **393**, e166095. https://doi.org/10.1136/bmj-2026-166095

[6] European Centre for Disease Prevention and Control (2026) Ebola Disease Outbreak in the Democratic Republic of the Congo and Uganda. https://www.ecdc.europa.eu/en/ebola-outbreak-democratic-republic-congo-and-uganda

[7] Wellcome Trust (2026) The 2026 Bundibugyo Ebola Outbreak: Why R&D Investment Matters. PreventionWeb.

[8] Edward, M., Muhigi, S., Mundua, J. and Ally, A. (2025) Resurgence of Ebola in Uganda: Response Strategies, Lessons Learned, and Future Directions. *Health Science Reports*, **8**, e70967. https://doi.org/10.1002/hsr2.70967

[9] International Organization for Migration (2026) Ebola Response Must Cross Borders Faster than the Virus, IOM Warns.

[10] Shen, L., Song, J., Zhou, Y., Yuan, X., Seery, S., Fu, T., *et al.* (2025) Assessing the Ecological Resilience of Ebola Virus in Africa and Potential Influencing Factors Based on a Synthesized Model. *PLOS Neglected Tropical Diseases*, **19**, e0012843. https://doi.org/10.1371/journal.pntd.0012843

[11] Baluma Didier, L., Jude, L.L., Franck, E.I., Wang, H. and Wang, X. (2024) Spatial Modeling and Ecological Suitability of Ebola Virus Disease in Africa. *PLOS ONE*, **19**, e0311936. https://doi.org/10.1371/journal.pone.0311936

[12] Jiang, S., Wang, K., Li, C., Hong, G., Zhang, X., Shan, M., *et al.* (2017) Mathematical Models for Devising the Optimal Ebola Virus Disease Eradication. *Journal of Translational Medicine*, **15**, Arti8cle No. 124. https://doi.org/10.1186/s12967-017-1224-6

[13] Legrand, J., Grais, R.F., Boelle, P.Y., Valleron, A.J. and Flahault, A. (2006) Understanding the Dynamics of Ebola Epidemics. *Epidemiology and Infection*, **135**, 610-621. https://doi.org/10.1017/s0950268806007217

[14] Colizza, V. and Vespignani, A. (2008) Epidemic Modeling in Metapopulation Systems with Heterogeneous Coupling Pattern: Theory and Simulations. *Journal of Theoretical Biology*, **251**, 450-467. https://doi.org/10.1016/j.jtbi.2007.11.028

[15] Colizza, V., Pastor-Satorras, R. and Vespignani, A. (2007) Reaction-Diffusion Processes and Metapopulation Models in Heterogeneous Networks. *Nature Physics*, **3**, 276-282. https://doi.org/10.1038/nphys560

[16] Chowell, G., Hengartner, N.W., Castillo-Chavez, C., Fenimore, P.W. and Hyman, J.M. (2004) The Basic Reproductive Number of Ebola and the Effects of Public Health Measures: The Cases of Congo and Uganda. *Journal of Theoretical Biology*, **229**, 119-126. https://doi.org/10.1016/j.jtbi.2004.03.006

[17] Chowell, G. and Nishiura, H. (2014) Transmission Dynamics and Control of Ebola Virus Disease (EVD): A Review. *BMC Medicine*, **12**, Article No. 196. https://doi.org/10.1186/s12916-014-0196-0

[18] Asiteza, R. (2026) Uganda Temporarily Shuts DRC Border as Ebola Cases Rise. Daily Express Uganda.

[19] Brainard, J., Hooper, L., Pond, K., Edmunds, K. and Hunter, P.R. (2015) Risk Factors for Transmission of Ebola or Marburg Virus Disease: A Systematic Review and Meta-Analysis. *International Journal of Epidemiology*, **45**, 102-116. https://doi.org/10.1093/ije/dyv307

[20] Wamala, J.F., Lukwago, L., Malimbo, M., Nguku, P., Yoti, Z., Musenero, M., *et al.*

(2010) Ebola Hemorrhagic Fever Associated with Novel Virus Strain, Uganda, 2007-2008. *Emerging Infectious Diseases*, **16**, 1087-1092. https://doi.org/10.3201/eid1607.091525

[21] Dowell, S., Mukunu, R., Ksiazek, T., Khan, A., Rollin, P. and Peters, C.J. (1999) Transmission of Ebola Hemorrhagic Fever: A Study of Risk Factors in Family Members, Kikwit, Democratic Republic of the Congo, 1995. *The Journal of Infectious Diseases*, **179**, S87-S91. https://doi.org/10.1086/514284

[22] MacNeil, A., Farnon, E.C., Wamala, J., Okware, S., Cannon, D.L., Reed, Z., *et al.* (2010) Proportion of Deaths and Clinical Features in Bundibugyo Ebola Virus Infection, Uganda. *Emerging Infectious Diseases*, **16**, 1969-1972. https://doi.org/10.3201/eid1612.100627

[23] Institut National de Santé Publique (INSP-DRC) (2026) SitRep N˚30/MVB_13/06/2026. Centre des Opérations d'Urgences de Santé Publique (COUSP-DRC).

[24] James, G., Witten, D., Hastie, T. and Tibshirani, R. (2023) An Introduction to Statistical Learning: with Applications in Python. Springer. https://doi.org/10.1007/978-3-031-38747-0

Appendix A. Justification for Estimating Beta from Sparse Data

Let $C_{\text{obs}}(t_i)$ denote the observed cumulative number of cases at observation times t_i, $i = 1, \cdots, n$, and let $C(t_i; \beta)$ denote the corresponding model prediction obtained from the SEIRD system.

To track cumulative infections, an additional state variable $C(t)$ was introduced into the model, satisfying $\frac{\mathrm{d}C}{\mathrm{d}t} = \sigma E$, with initial condition $C(0) = I_0 + R_0 + D_0$. Since σE represents the rate at which exposed individuals become infectious, the variable $C(t)$ records the cumulative number of individuals who have entered the infectious class.

Table A1. Initial seeding summary and case mappings at $t = 0$.

Location/Category	Infected (I)	Recovered (R)	Deceased (D)	Exposed (E)
Kampala	9	4	2	Modulated via Eq. 12
Wakiso	5	1	0	Modulated via Eq. 12
Global Mapping	14 (Imp), 7 (Loc)	Derived from mapping	Derived from mapping	-

Table A2. Distance matrix (d_{ri} in km) from DRC epicenters to ugandan destination districts.

Origin (r)	Kampala	Ntoroko	Wakiso	Arua	Kasese	Koboko	Nebbi	Fort Portal	Kisoro	Hoima
Bunia	712.213	486.107	716.743	1252.632	337.506	1286.659	1140.547	412.697	624.211	899.747
Mongbwalu	786.819	560.712	791.348	1327.237	412.111	1361.264	1215.153	487.303	698.817	974.352
Beni	515.415	289.308	519.944	1055.834	140.707	1089.860	943.749	215.899	427.208	702.949
Butembo	567.119	341.012	571.648	1107.538	192.411	1141.564	995.453	267.603	375.776	754.653
Goma	587.773	552.714	592.302	1128.191	404.113	1162.218	1016.107	479.305	102.740	775.306

Source: Road network data obtained from ArcGIS Online through ArcGIS Catalog; map created by the author in ArcGIS Pro.

Table A3. Ugandan district populations as of June 13, 2026.

District	Population
Kampala	1,875,834
Ntoroko	114,859
Wakiso	3,397,565
Arua	159,491
Kasese	847,027
Koboko	271,655
Nebbi	299,185
Fort Portal City	135,702
Kisoro	431,175
Hoima	257,430

Table A4. 2026 Uganda confirmed cases by (I) reporting day as of 2024.

Day	Date	Cases
0	15 May	3
1	17 May	0
2	19 May	0
3	21 May	0
4	23 May	3
5	25 May	2
6	27 May	0
7	29 May	2
8	31 May	2
9	02 Jun	4
10	04 Jun	1
11	06 Jun	4
12	08 Jun	0
13	10 Jun	0

Table A5. Road distance matrix $\left(d_{ij}\right)$ (km) between selected Ugandan districts.

Origin	Kampala	Ntoroko	Wakiso	Arua	Kasese	Koboko	Nebbi	FortPortal	Kisoro	Hoima
Kampala	0.000000	371.341760	16.469835	547.622587	422.560754	581.649233	435.537998	294.392854	485.959207	199.473922
Ntoroko	371.341760	0.000000	374.538744	910.427866	152.567003	944.454512	798.343277	79.631643	450.910883	475.273254
Wakiso	15.884652	375.290170	0.000000	555.978190	427.239096	590.004835	443.893601	298.341264	490.637549	183.767918
Arua	546.975137	911.112375	556.279928	0.000000	963.061301	65.316124	101.501152	834.163469	1026.459754	565.684231
Kasese	422.538038	152.440027	427.067656	962.956778	0.000000	996.983424	850.872189	79.030802	302.319365	474.672337
Koboko	581.024027	945.161265	590.328818	65.316214	997.110190	0.000000	146.133478	868.212358	1060.508643	599.733120
Nebbi	434.890548	799.027786	444.195340	101.501152	850.976712	146.111235	0.000000	722.078880	914.375165	453.599642
FortPortal	294.352178	79.676984	297.635149	833.524271	79.108637	867.550917	721.439682	0.000000	377.452517	398.369659
Kisoro	485.925417	450.866655	490.455035	1026.344157	302.265799	1060.370803	914.259568	377.457430	0.000000	673.459122
Hoima	198.892517	475.322342	183.771694	565.730534	474.753964	599.757180	453.645945	398.373436	673.645413	0.000000

Source: Road network data obtained from ArcGIS Online through ArcGIS Catalog; map created by the author in ArcGIS Pro.